Nanofabrication (2024)
https://doi.org/10.37819/nanofab.9.1783

RESEARCH ARTICLE

Sputtering Deposition of ZnO Thin Films for Photocatalytic Hydrogen Production: Perspectives on Upscaling

Iván R. Rodríguez[a*], Andrés Galdámez-Martínez[b*], Carlos Ramos[c*], Guillermo Santana[c], Agileo Hernández Gordillo[c], Ateet Dutt[c]
[a]Facultad de Ciencias, Universidad Nacional Autónoma de México, C.P. 04510, México City, México.
[b]Departamento de Física, Universidad Autónoma Metropolitana Unidad Iztapalapa, C.P. 09340, México City, México.
[c]Departamento de Materiales de Baja Dimensionalidad, Instituto de Investigaciones en Materiales Universidad Nacional Autónoma de México. C.P. 04510, Mexico City, Mexico.
***Corresponding author's Email**: adutt@iim.unam.mx, agileohg@iim.unam.mx
*Equal contribution

Abstract

This study presents the successful implementation of ZnO thin films (denoted as z01, z02, and z03) through magnetron sputtering in the photocatalytic production of hydrogen using a low-intensity UV source (3 mW cm^{-2}). The one-step synthesis process demonstrates simplicity and scalability. The deposited coatings, with thicknesses ranging from 62 to 209 nm, exhibit a hexagonal crystalline structure and display visible luminescence in the yellow-red range, attributed to point defects in the ZnO lattice. Among the samples, z03 (62 nm in thickness) exhibited the most promising performance in photocatalytic hydrogen production, achieving a rate of (5387.2 ± 151.6) µmol g^{-1} h^{-1} when utilizing methanol as a hole scavenger. These findings hold great potential for upscaling such coatings in energy harvesting applications. The present work opens new avenues for efficient and scalable hydrogen production, contributing to improving clean energy technologies.

Keywords: ZnO thin films, photocatalysis, hydrogen production, magnetron sputtering, energy harvesting

Article history:

Received: 16-Sept-2023

Revised: 22-Dec-2023

Accepted: 26-Jan-2024

1. Introduction

In pursuing sustainable energy sources and environmental improvement, photocatalytic hydrogen production through water splitting has emerged as a promising avenue(Toe et al., 2022). Hydrogen, as a clean and high-energy-density fuel, holds an immense pledge to meet the world's future energy needs while substantially reducing greenhouse gas emissions(Arora & Mishra, 2019). Using solar energy and materials semiconductors to drive this chemical reaction offers a solution to growing global energy demands and the urgent need to mitigate climate change. Among the various materials used as photocatalysts, zinc oxide (ZnO) has gained significant attention due to its inherent optoelectronic properties, including strong photoactivity, chemical stability, and cost-effectiveness (Sun et al., 2023).

Over the years, extensive research efforts have been dedicated to exploring various methods for synthesizing ZnO-based photocatalyst materials, such as sol-gel(Mahdavi & Talesh, 2017), hydrothermal(Sansenya et al., 2022), and chemical vapor deposition(Jiamprasertboon et al., 2019). These investigations have highlighted ZnO's potential as a photocatalyst, with notable progress in enhancing its photocatalytic activity through surface modification, defect engineering, and size control(Kegel et al., 2018). However, producing ZnO photocatalyst materials at a large scale with precisely engineered properties remains a challenge, hindering their practical use in large-scale photocatalytic hydrogen production(Kuspanov et al., 2023).

Recognizing the pivotal role that hydrogen plays in the transition to a sustainable energy landscape, the need for a scalable and efficient method for ZnO photocatalyst synthesis becomes evident. Therefore, a comprehensive exploration of innovative approaches to produce efficient ZnO-based photocatalysts is essential, aligning with the sustainable transition framework endorsed by the global scientific community.

Thin ZnO films deposited by the magnetron sputtering technique offer distinct advantages, including precise control over film thickness, excellent uniformity, and compatibility with diverse substrates, making it an ideal candidate for large-scale production(Cheng et al., 2023). By employing this technique, we address the critical challenge of scalability and aim to bridge the gap between fundamental research and practical applications in photocatalytic hydrogen production.

This study focuses on creating thin ZnO films through magnetron sputtering and their application in the photocatalytic production of hydrogen, contributing to the field of sustainable energy conversion. The ZnO films, ranging in thickness from 209 to 62 nm, exhibited a hexagonal crystalline structure (crystallite sizes 11-13 nm). Notably, all synthesized coatings demonstrated visible luminescence in the yellow-red spectral region, attributed to point defects in the ZnO lattice. Regarding the photocatalytic performance, the highest observed efficiency in hydrogen production was 5387.2 ± 151.6 µmol g^{-1} h^{-1}, achieved when methanol was employed as a hole scavenger agent. Therefore, the present article outlines the experimental procedures and scalable approach for synthesizing thin ZnO films, characterization techniques, and small-scale photocatalytic performance assessments. Our findings underscore the potential of these films as efficient photocatalysts for hydrogen evolution from water splitting, paving the way for their integration into sustainable and scalable hydrogen production systems. Given the global commitment to mitigating climate change and transitioning to clean energy sources, the outcomes of this study have significant implications for advancing state-of-the-art sustainable energy conversion technologies.

2. Experimental methodology

2.1. ZnO thin film deposition

Thin films of ZnO were synthesized using the direct current (DC) magnetron sputtering technique on (111) crystalline silicon wafers (2”). Substrate cleaning was carried out by immersion in sequential ultrasonic baths containing isopropanol, acetone, and deionized water for 5 minutes, followed by drying with pressurized nitrogen. An additional cleaning step involving an HF:HNO_3:H_2O acidic solution with proportions of 1 vol%:10 vol%:100 vol% was used to eliminate impurities from the substrate surfaces. Subsequently, the wafers were placed inside a commercial sputtering equipment (Intercovamex ®) chamber utilizing a ZnO (99.99%) target as the erosion cathode. A base pressure of (9.99 ± 0.5) x10^{-5} mbar was achieved using a high-vacuum system. Subsequently, a flow of 30 sccm of Ar (99.999%) was introduced to attain a working pressure of (1.20 ± 0.06) x10^{-2} mbar. Film deposition was conducted with a power input of 40 W for 60 minutes. This process resulted in the deposition of thin ZnO films across the entire surface of the silicon wafer. Finally, the wafer was laser-cut into samples of identical area (1.57 ± 0.05) cm^2.

2.2. Characterization techniques

For the morphological characterization of the deposited films, a scanning electron microscope JEOL 7600 was employed. The crystalline structure was ascertained using a Rigaku Ultima IV X-ray diffractometer in its grazing incidence mode. Spectra of specular reflectance from the obtained films were determined utilizing a Filmetrics F10-RT-UV ultraviolet-visible spectrometer. Additionally, the photoluminescence emission spectra of the films were measured using a He-Cd laser (λ=325 nm) and an Acton Spectra Pro 2500i spectrometer.

2.3. Photocatalytic trials

The experimental procedure was adapted from(Cerezo et al., 2022) for the hydrogen evolution reaction measurements. A custom-made 30 mL Pyrex reactor containing a water-ethanol (1 vol%:1 vol% ratio) solution and 8 ZnO thin films (total area of 12.6 cm^2) attached to the inner walls of the reactor were employed. Illumination was achieved through a high-pressure mercury pen-ray lamp emitting at 254 nm with an intensity I_0 = 3 $mWcm^{-2}$, measurement at 2 cm by using SRI-2000 Spectra Light Meter Allied Scientific Pro). This lamp was encapsulated within a quartz tube and submerged in the aqueous solution. **Figure SI 1** presents the reactor schematic employed in the photocatalytic trials.

Hydrogen production was quantified via gas chromatography, employing a Shimadzu GC-2014 gas chromatograph equipped with a thermal conductivity detector and a 5A column molecular sieve measuring 30 meters in length, 0.35 mm in internal diameter, and 50 mm in outer diameter. Before the ZnO film H_2 production measurements, the photolysis contribution was determined using only the ethanol-water mixture under the described photocatalytic conditions. This was later used as a baseline correction to the hydrogen evaluation performance with the photocatalyst films.

3. Results

The ZnO thin film samples deposited on silicon (Si) substrates are visually represented in **Fig. 1a**. The concentric rings of varying colors arise from using a static magnetron and target within the sputtering device, consequently inducing a gradient in material deposition. The coloration of these rings corresponds to the thickness of the thin film, with inner circles being inherently thicker. This phenomenon is attributed to the spatial distribution of the plasma, resulting in a more substantial material deposition towards the center and a gradual reduction as the rings approach the periphery. This leads to thinner deposits at the outer edges of the rings. To ensure the morphological and structural properties of the deposited ZnO thin films, the silicon wafer was carefully sectioned into batches based on the rings' color, resulting in three distinct groups. These groups were denoted as z01 (centermost), z02 (midway towards the borders), and z03 (nearest to the ends of the wafer), as represented in **Fig. 1b**. Each sample within these groups possessed uniform dimensions, measuring 1.25 x 1.25 cm, resulting in a total surface area of 1.5625 cm².

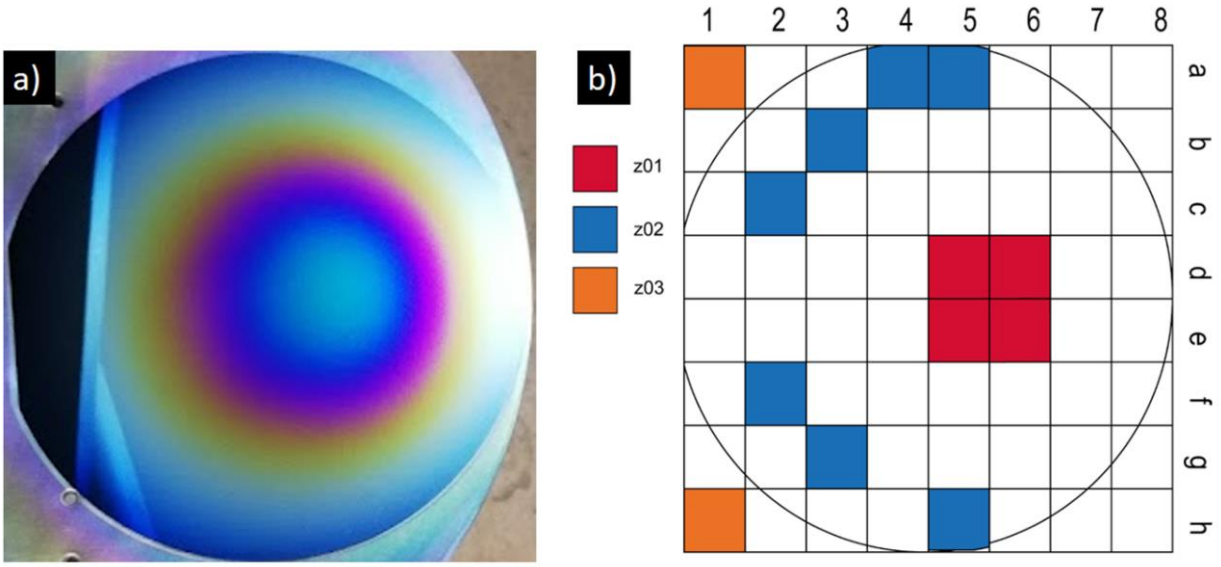

Fig. 1. a) Si substrate after ZnO thin film deposit by magnetron sputtering. b) Cuts made to the substrate and selection of samples for every batch.

Afterward, scanning electron microscope (SEM) transverse images were captured from representative samples within each batch, as depicted in **Fig. 2 (a-c)**. These images exhibit a discernible contrast between the Si substrate and the ZnO thin film, allowing for precise measurements of the ZnO deposit thickness. The data was meticulously analyzed using ImageJ software, revealing average thicknesses of (205 ± 4) nm, (113 ± 5) nm and (63 ± 1) nm for z01, z02 and z03, respectively.

Fig. 2d depicts the grazing incidence X-ray diffraction (GIXRD) patterns of the z01, z02, and z03 samples, wherein crystal structure identification was performed with Match! 3 software. The observed peaks, therefore, correspond to the hexagonal wurtzite structure of ZnO, characterized by lattice constants a = b = 3.25 Å and c = 5.22 Å according to the JCPDS database entry #96-101-1260(Akay et al., 2018). It can be noticed that the most intense reflection corresponds to the (002) plane, which characterizes the crystal growth in the *c*-direction. The determination of crystallite size (D) was carried out using the Scherrer formula(Mishra et al., 2012) and considering the full width at half-maximum (β) of the (002) peak, which shows a broadening due to crstallite dimensions $D = \frac{K\lambda}{\beta \cos\theta}$

In which a constant (K = 0.9), the X-ray wavelength used in X-ray diffraction (Cu Kα = 0.15418 Å), and the Bragg angle (θ) are the other parameters involved in the former calculation. Consequently, the crystallite sizes for the z01, z02, and z03 samples are determined to be 13 nm (β=0.71), 11 nm (β=0.74), and 11 nm (β=0.76), respectively. The phenomenon of thinner films exhibiting smaller crystallite sizes can be attributed to the quantity of material present.

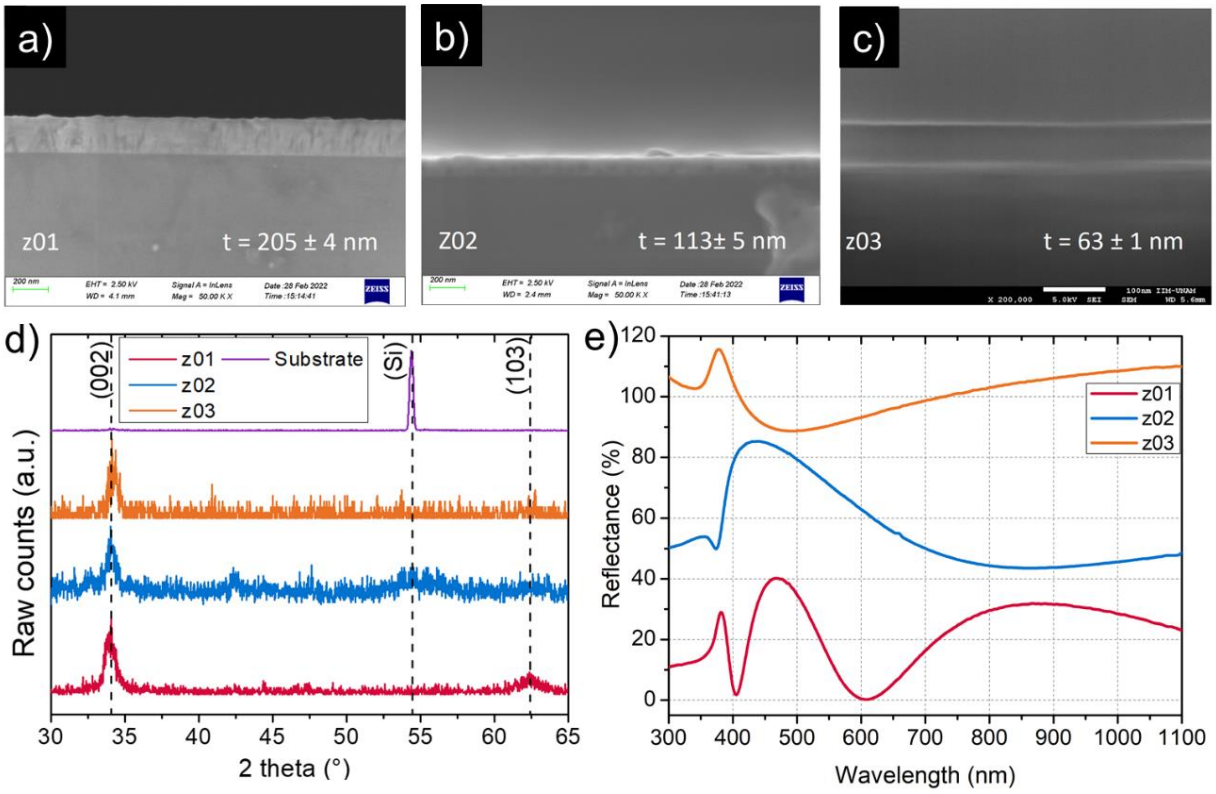

Fig. 2. (a-c) Transversal SEM images showing the average thickness and standard deviation of ZnO coatings deposited by the magnetron sputtering technique. (d) X-ray diffraction patterns in grazing angle configuration (GIXRD) of ZnO thin films deposited on Si substrate. Monocrystalline substrate diffractogram included as a reference. (e) UV-visible specular reflectance spectroscopy of z01-z03 samples.

In cases with less material and an equivalent deposition duration, crystallites are afforded a smaller opportunity for growth before encountering a limiting boundary. This dynamic allows for the observed decrease in crystallite size. In **Fig. 2d**, the reflection of the plane (103) is also perceptible for sample z01. This observation is influenced by the use of grazing incidence angle radiation during acquiring these measurements. Because of this experimental configuration, the diffraction condition corresponding to the Bragg angle ($2\theta = 62.4^{o}$) coincidentally aligns with crystals characterized by a preferred growth orientation orthogonal to the substrate plane. To expand upon this diffraction condition with the crystallographic orientation of nanostructured ZnO coatings as ascertained through (GIXRD), a comprehensive elucidation is available in previous reports(Galdámez-Martínez et al., 2022).

Fig. 2e presents the specular reflectance spectra of the coatings. There is a substantial difference in the optical characteristics of the three systems. The disparity in sample thickness is further substantiated by examining the position and quantity of interference fringes, wherein thicker films (z01) exhibit a more significant number of oscillations across the measured spectral range compared to their thinner counterparts (z03). This straightforward characterization method facilitated the identification and subsequent selection of film batches possessing uniform thickness and structural attributes across the entirety of the silicon wafer surface.

Furthermore, the luminescent properties of the synthesized films were examined via room-temperature photoluminescence spectroscopy (**Fig. 3a**). As depicted in this figure, the emission spectra exhibit distinct features contingent upon the film thickness, manifesting shifts in both the dominant emission peaks maxima (z01: 602 nm,

z02: 610 nm, and z03: 588 nm) and FHWM (z01:61 nm, z02:151 nm, and z03:179 nm). Consequently, to elucidate the intra-band recombination centers linked to point defects within the ZnO lattice that participate in the material's emission, a deconvolution process was executed employing Gaussian curves. With the deconvolution process of the spectra, all samples show a peak at the violet/purple region (2.95-3.07 eV), which is either associated with Zn vacancy (V_{Zn}) or zinc interstitials (Shen et al., 2022) and peaks in the yellow/red region (2.10-1.90 eV) attributed to oxygen interstitial (O_i)(Musavi et al., 2019). These recombination centers adequately account for the emission in the z01 and z02 coatings.

Nevertheless, through the spectrum fitting process for the z03 sample, additional centers contributing to the material's emission were identified. In this instance, the sample exhibits centers at 2.65 eV and 2.17 eV, which have been previously attributed in reports to extended zinc interstitials (ex-Zn_i)(Galdámez-Martínez et al., 2023) and V_OZn_i(Alvi et al., 2010) complex, respectively. Although the unequivocal assignment of these defects remains a subject of ongoing debate in the literature(Wang et al., 2018), the assertion that a higher abundance of defects is associated with the emission of the thinner ZnO films synthesized in this study is compelling. This assertion is substantiated by the broad, yellow-centered emission observed in the photoluminescence spectra compared to the other two systems.

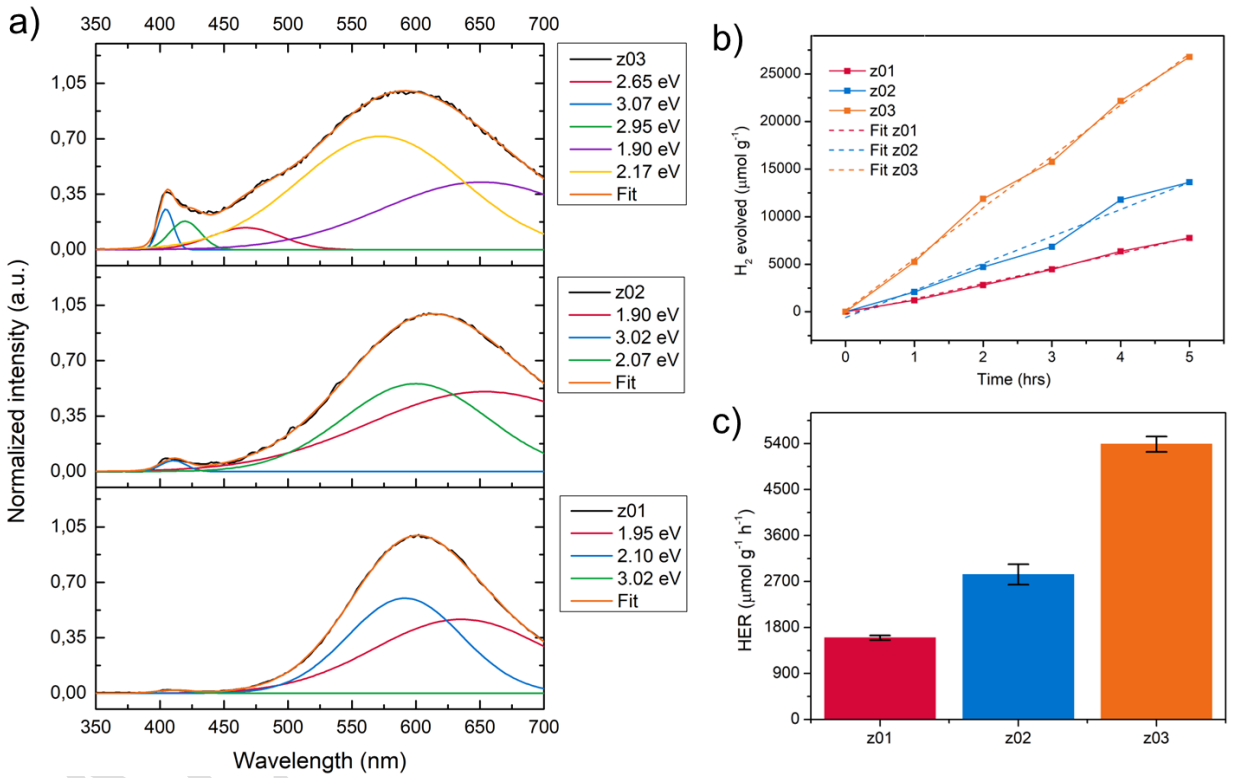

Fig. 3. (a) Room temperature photoluminescence spectra of ZnO thin films (black). Gaussian deconvolution curves (color). (b) Photocatalytic hydrogen evolution over time of the ZnO photocatalyst thin films (z01, z02, z03) from a 30 ml H_2O (50 % vol): CH_3OH (50 % vol) solution under 254 nm Hg lamp irradiation (2.2 mW cm^{-2}). (c) Photocatalytic hydrogen evolution rates of z01, z02, and z03 ZnO thin films.

In addition to the morphological, optical, and structural characterizations conducted on the synthesized ZnO coatings, assessments were also performed to evaluate their efficacy as photocatalyst materials in the context of hydrogen generation from an aqueous solution containing ethanol as a hole scavenger agent. **Fig. SI 2** presents the raw data measurements without photolysis baseline correction, determined via CG employing films from the batches with similar thickness and optostructural characteristics (i.e., z01, z02, z03). To ascertain the hydrogen production efficiency of the analyzed coatings, estimating the deposited mass of ZnO onto the silicon substrates was imperative, considering the known film thickness values and the area utilized. Consequently, our calculations indicate that the approximate masses of the z01 to z03 coatings fall within the 1.4 to 0.4 mg range.

Considering these considerations, the photogenerated hydrogen evolution of the ZnO coatings, as displayed in **Fig. 3b**, was determined. It is observed that all coatings exhibit the ability to generate hydrogen from water in the presence of ethanol. Under the applied conditions, it is noted that the sample demonstrating the highest hydrogen production rate is z03 (5387.2 ± 151.6 µmol g^{-1} h^{-1}) In contrast, the other two samples display comparatively lower efficiencies (z01: 1597.6 ± 47.0 µmol g^{-1} h^{-1} and z02: 2836.9 ± 198.4 µmol g^{-1} h^{-1}), which tendency is attributed to the diminished quantity of photocatalytic material employed in the experimental setup (**Fig. 3c**). Additionally, when calculating the hydrogen evolution rates (HER) about the surface area employed, the following values are obtained: z01 = 0.184 µmol cm^{-2} h^{-1}, z02 = 0.180 µmol cm^{-2} h^{-1} and z03 = 0.190 µmol $cm^{-2}h^{-1}$, which are quite close from each other. Hence, although somewhat rudimentary, the approaches utilized to assess the hydrogen production efficiency of the mass of the synthesized coatings distinctly elucidate the variations in the photocatalytic film performances based on their thickness. It is worth emphasizing that the z03 sample exhibits superior hydrogen production performance and contains a higher concentration of point defects, as previously discussed in the photoluminescence analysis. Consequently, their enhanced photocatalytic performance might be attributed to the efficient involvement of these energy levels in charge carrier separation, thus facilitating an increase in the proton reduction rate for hydrogen production.

Table 1. Outcomes documented in the literature regarding the photocatalytic efficacy for hydrogen production employing thin semiconductor films.

Material	**Hydrogen evolution ratio**	**Ref**
ZnO thin films	(5387.2 ± 151.6) µmol g^{-1} h^{-1}	This work
Titania (Anatase: Rutile) thin films	2.28 mmol g^{-1} h^{-1}	(Nalajala et al., 2019)
Ag-doped ZnO thin films	10 µmol h^{-1}	(Rabell et al., 2021)
PbS/ZnO thin films	7.38 µmol cm^{-2} h^{-1}	(Carrasco-Jaim et al., 2017)
Fe-doped TiO_2 thin films	15.5 µmol h^{-1}	(Dholam et al., 2009)
Amorphous TiO_2 thin films	(0.46 ± 0.66) mmol g^{-1} h^{-1}	(Shwetharani et al., 2020)

Finally, **Table 1** compares the reported results of this study with those derived from analogous investigations, illustrating the efficacy of thin semiconductor film systems for the photocatalytic production of hydrogen. Notably, our results present superior performance to TiO_2-based systems under similar operating conditions (Nalajala et al., 2019). Nevertheless, in a considerable number of studies employing thin films, the comparability of results among different authors is impeded by variations in measurement conditions such as reactor configurations and irradiation sources. This intricacy underscores the challenge of achieving a direct, unbiased comparison across diverse scholarly contributions, warranting further attention to enhance the objectivity of assessments in this research area.

4. Conclusions

This research successfully deposited ZnO thin films (denoted as z01, z02, and z03) using the magnetron sputtering technique for photocatalytic hydrogen production under low-intensity UV light (3 $mWcm^{-2}$). The one-step synthesis process proved to be both straightforward and scalable, allowing the production of ZnO thin films across the entire surface of a two-inch silicon wafer.

The obtained coatings, with thicknesses ranging from 209 to 62 nm, exhibited a hexagonal crystalline structure and crystallite sizes between 11 and 13 nm, as determined by the Scherrer formula. Ultraviolet-visible reflectance spectroscopy facilitated the successful correlation of film thickness with a readily monitorable signal, thus enabling the grouping of films with similar optostructural characteristics.

All synthesized coatings exhibited visible luminescence in the yellow-red region, attributed to point defects in the ZnO lattice, particularly oxygen interstitials. Notably, the Z03 sample (63 nm) demonstrated the highest performance in photocatalytic hydrogen production (5387.2 ± 151.6 µmol g^{-1} h^{-1}) when utilizing methanol as a hole scavenger agent. These results hold significant promise for the scalability of such coatings in energy harvesting applications.

In summary, implementing ZnO thin films via magnetron sputtering for photocatalytic hydrogen production, especially the z03 sample, has exhibited encouraging results. The simplicity and scalability of the one-step synthesis process, coupled with the distinct optical and structural properties of the films, make them a viable candidate for applications in energy harvesting.

Acknowledgments

A.G.M acknowledges CONACyT Grant CVU 860916. A.D. thanks the project PAPIIT-DGAPA-UNAM IA100123. G. The authors would also like to thank Alejandro Pompa, Oscar Luna, and Celic Martínez for their technical assistance. Special thanks to the "Laboratorio Universitario de Microscopía Electrónica" (LUME) and Josue Esau Romero Ibarra for their technical support.

References

Akay, S. K., Sarsıcı, S., & Kaplan, H. K. (2018). Determination of electrical parameters of ZnO/Si heterojunction device fabricated by RF magnetron sputtering. *Optical and Quantum Electronics*, *50*(10). https://doi.org/10.1007/s11082-018-1635-5

Alvi, N. H., Willander, M., & Nur, O. (2010). The effect of the post-growth annealing on the electroluminescence properties of n-ZnO nanorods/p-GaN light emitting diodes. *Superlattices and Microstructures*, *47*(6), 754–761. https://doi.org/10.1016/j.spmi.2010.03.002

Arora, N. K., & Mishra, I. (2019). United Nations Sustainable Development Goals 2030 and environmental sustainability: race against time. *Environmental Sustainability*, *2*(4), 339–342. https://doi.org/10.1007/s42398-019-00092-y

Carrasco-Jaim, O. A., Ceballos-Sanchez, O., Torres-Martínez, L. M., Moctezuma, E., & Gómez-Solís, C. (2017). Synthesis and characterization of PbS/ZnO thin film for photocatalytic hydrogen production. *Journal of Photochemistry and Photobiology A: Chemistry*, *347*, 98–104. https://doi.org/10.1016/j.jphotochem.2017.07.016

Cerezo, L., Valencia G., K., Hernández-Gordillo, A., Bizarro, M., Acevedo-Peña, P., & Rodil, S. E. (2022). Increasing the H2 production rate of ZnS(en)x hybrid and ZnS film by photo exfoliation process. *International Journal of Hydrogen Energy*, *47*(53), 22403–22414. https://doi.org/10.1016/j.ijhydene.2022.05.049

Cheng, P., Döll, J., Romanus, H., Wang, H., van Aken, P. A., Wang, D., & Schaaf, P. (2023). Reactive Magnetron Sputtering of Large-Scale 3D Aluminum-Based Plasmonic Nanostructure for Both Light-Induced Thermal Imaging and Photo-Thermoelectric Conversion. *Advanced Optical Materials*, *11*(6). https://doi.org/10.1002/adom.202202664

Dholam, R., Patel, N., Adami, M., & Miotello, A. (2009). Hydrogen production by photocatalytic water-splitting using Cr- or Fe-doped TiO2 composite thin films photocatalyst. *International Journal of Hydrogen Energy*, *34*(13), 5337–5346. https://doi.org/10.1016/j.ijhydene.2009.05.011

Galdámez-Martínez, A., Armenta-Jaime, E., Zayas-Bazán, P., Santana Rodriguez, G., Sánchez-Aké, C., Novelo-Peralta, O., Mishra, Y. K., Kaushik, A. K., & Dutt, A. (2023). Controlling Green-to-Blue Luminescence in Multidimensional ZnO Interfaces: Mechanistic Insights. *ACS Applied Optical Materials*. https://doi.org/10.1021/acsaom.3c00180

Galdámez-Martínez, A., Dutt, A., Jain, M., Bazán-Díaz, L., Santana, G., Méndez-Blas, A., & de Melo, O. (2022). Decay emission study of ZnO nanostructures obtained by low-pressure vapor transport technique. *Applied Surface Science Advances*, *12*(September), 100334. https://doi.org/10.1016/j.apsadv.2022.100334

Jiamprasertboon, A., Dixon, S. C., Sathasivam, S., Powell, M. J., Lu, Y., Siritanon, T., & Carmalt, C. J. (2019). Low-Cost One-Step Fabrication of Highly Conductive ZnO:Cl Transparent Thin Films with Tunable Photocatalytic

Properties via Aerosol-Assisted Chemical Vapor Deposition. *ACS Applied Electronic Materials*, *1*(8), 1408–1417. https://doi.org/10.1021/acsaelm.9b00190

Kegel, J., Povey, I. M., & Pemble, M. E. (2018). Zinc oxide for solar water splitting: A brief review of the material's challenges and associated opportunities. *Nano Energy*, *54*(October), 409–428. https://doi.org/10.1016/j.nanoen.2018.10.043

Kuspanov, Z., Bakbolat, B., Baimenov, A., Issadykov, A., Yeleuov, M., & Daulbayev, C. (2023). Photocatalysts for a sustainable future: Innovations in large-scale environmental and energy applications. *Science of The Total Environment*, *885*, 163914. https://doi.org/10.1016/j.scitotenv.2023.163914

Mahdavi, R., & Talesh, S. S. A. (2017). Sol-gel synthesis, structural and enhanced photocatalytic performance of Al doped ZnO nanoparticles. *Advanced Powder Technology*, *28*(5), 1418–1425. https://doi.org/10.1016/j.apt.2017.03.014

Mishra, S. K., Srivastava, R. K., & Prakash, S. G. (2012). ZnO nanoparticles: Structural, optical and photoconductivity characteristics. *Journal of Alloys and Compounds*, *539*, 1–6. https://doi.org/10.1016/j.jallcom.2012.06.024

Musavi, E., Khanlary, M., & Khakpour, Z. (2019). Red-orange photoluminescence emission of sol-gel dip-coated prepared ZnO and ZnO:Al nano-crystalline films. *Journal of Luminescence*, *216*(February). https://doi.org/10.1016/j.jlumin.2019.116696

Nalajala, N., Patra, K. K., Bharad, P. A., & Gopinath, C. S. (2019). Why the thin film form of a photocatalyst is better than the particulate form for direct solar-to-hydrogen conversion: A poor man's approach. *RSC Advances*, *9*(11), 6094–6100. https://doi.org/10.1039/c8ra09982k

Rabell, G. O., Cruz, M. R. A., & Juárez-Ramírez, I. (2021). Hydrogen production of ZnO and ZnO/Ag films by photocatalysis and photoelectrocatalysis. *Materials Science in Semiconductor Processing*, *134*. https://doi.org/10.1016/j.mssp.2021.105985

Sansenya, T., Masri, N., Chankhanittha, T., Senasu, T., Piriyanon, J., Mukdasai, S., & Nanan, S. (2022). Hydrothermal synthesis of ZnO photocatalyst for detoxification of anionic azo dyes and antibiotic. *Journal of Physics and Chemistry of Solids*, *160*. https://doi.org/10.1016/j.jpcs.2021.110353

Shen, H., Shi, X., Wang, Z., Hou, Z., Xu, C., Duan, L., Zhao, X., & Wu, H. (2022). Defects control and origins of blue and green emissions in sol-gel ZnO thin films. *Vacuum*, *202*(March), 111201. https://doi.org/10.1016/j.vacuum.2022.111201

Shwetharani, R., Chandan, H. R., Sakar, M., Balakrishna, G. R., Reddy, K. R., & Raghu, A. V. (2020). Photocatalytic semiconductor thin films for hydrogen production and environmental applications. *International Journal of Hydrogen Energy*, *45*(36), 18289–18308. https://doi.org/10.1016/j.ijhydene.2019.03.149

Sun, Y., Zhang, W., Li, Q., Liu, H., & Wang, X. (2023). Preparations and applications of zinc oxide based photocatalytic materials. *Advanced Sensor and Energy Materials*, *2*(3), 100069. https://doi.org/10.1016/j.asems.2023.100069

Toe, C. Y., Pan, J., Scott, J., & Amal, R. (2022). Identifying Key Design Criteria for Large-Scale Photocatalytic Hydrogen Generation from Engineering and Economic Perspectives. *ACS ES&T Engineering*, *2*(6), 1130–1143. https://doi.org/10.1021/acsestengg.2c00030

Wang, J., Chen, R., Xiang, L., & Komarneni, S. (2018). Synthesis, properties and applications of ZnO nanomaterials with oxygen vacancies: A review. *Ceramics International*, *44*(7), 7357–7377. https://doi.org/10.1016/j.ceramint.2018.02.013

Nanofabrication (2024)
https://doi.org/10.37819/nanofab.9.1783